The 8th IFToMM International Conference on Rotor Dynamics
September 12-15, 2010 / KIST, Seoul, Korea

NONLINEAR ROTORDYNAMICS OF VEHICLE TURBOCHARGERS: PARAMETERS AFFECTING SUB HARMONIC WHIRL FREQUENCIES AND THEIR JUMP

Luis San Andrés
Mast-Childs Professor
Texas A&M University
College Station, TX, USA

Arian Vistamehr
Research Assistant
Texas A&M University
College Station, TX, USA

ABSTRACT

Turbochargers (TCs) increase internal combustion engine power and efficiency in transportation vehicles. TC rotors are usually supported on engine oil lubricated floating ring bearings (FRBs) or semi-floating ring bearings (SFRBs), both inexpensive to manufacture. However, these bearing types are highly nonlinear and determine a complex rotordynamic behavior of the entire rotor-bearing system (RBS) which shows large amplitude sub harmonic motions, notable bifurcations, whirl frequency jumps, even mechanical hysteresis. Whirl frequency jump phenomenon is of concern due to the increased levels of TC induced noise generation. This paper details progress on assessing the effects of inlet oil conditions (pressure and temperature), imbalance distribution, and rotor acceleration on the TC RBS dynamic forced response. A fluid film bearing model is integrated into a FE rotordynamics model for numerical prediction of the TC linear and nonlinear (time transient) forced response. Since vehicle TCs operate at varying speed ranges, predictions are obtained for realistic shaft acceleration/deceleration conditions. Over most of its operating speed range, TC rotor nonlinear response predictions display two subsynchronous whirl frequencies ω_1 and ω_2 associated to rotor conical and cylindrical bending modes, respectively. At low shaft speeds ω_1 is present up to a threshold shaft speed (Ω_b) at which there is a whirl frequency jump to ω_2. Motions with the second whirl frequency may persist up to the highest shaft speeds, depending on the operating conditions. A single parameter variation study shows that reducing the oil supply pressure, and to a lesser extent, increasing the oil inlet temperature, brings the whirl frequency jump to occur at a lower threshold rotor speed (Ω_b). Hence, TC operation becomes noisier for operation at higher shaft speeds, $\Omega>\Omega_b$. Most notably, there is a pronounced hysteresis phenomenon, since as the rotor decelerates from its maximum speed, the threshold speed for the jump in whirl frequency is markedly distinct than when the rotor accelerates. Operation with the fastest rotor acceleration (deceleration) rate produces the strongest hysteresis. In addition, the rotor imbalance distribution greatly affects the location of the threshold speed Ω_b and the amplitude of total rotor motion.

INTRODUCTION

Turbochargers (TCs) increase both the efficiency and power of internal combustion engines (ICEs), also aiding to reducing ICE size and weight. TCs also improve air/fuel ratios for cleaner combustion, hence helping to reduce CO emissions [1]. Thus, passenger and commercial turbocharged vehicles, European and Asian in particular, have a lesser environmental impact than other vehicles. In the US personal transportation market, a turbocharged vehicle is presently welcomed as a green technology and not just a power boosting, luxury type mechanical component.

TCs are supported on engine oil lubricated bearings, floating and semi-floating. Low cost production and operation determines the choice of bearings. However, oil lubricated TCs typically are highly nonlinear systems evidencing complex rotordynamic response with multiple whirl frequencies –mainly sub harmonic, and showing whirl frequency jumps that result in increased levels of noise generation, thus affecting the mechanical reliability of the TC and its engine while also promoting passenger discomfort [2-8].

Figure 1 depicts a TC rotor supported on a semi-floating ring bearing system (SFRB). Oil, supplied through the center housing, flows into the compressor and turbine side bearings; each with two fluid films in series; an inner film separating the shaft from the ring inner side, and an outer film separating the ring outer side from the housing. A loose pin prevents the rotation of the floating ring. SFRBs offer lesser power losses that floating ring bearings [9]; and most importantly, allow for a compact rotor bearing system (RBS) where a single mechanical element integrates both radial and thrust bearings.

Until recently TC performance qualification involved rigorous testing, both costly and time consuming. The process often produced delays and severe economic losses. Hence, in 2001 a TC manufacturer established a long term effort with the author's laboratory to develop accurate and efficient virtual computational tools for prediction of TC nonlinear rotordynamic forced response [2-8]. Presently, the physics based computational model, experimentally benchmarked, has demonstrated a 70% cycle time reduction in new TC development with significant economic savings in product qualification and field verification [7].

San Andrés and Kerth [2] detail the elastohydrodynamic lubrication and thermal energy transport models for prediction of the forced performance of semi-floating and fully floating ring bearings and include predictions compared to measured film temperatures, power losses and ring rotational speeds. San Andrés *et al*. [5] observe that feed oil pressure exerts a significant side load on small TCs, account for the hydrostatic

load in the computational model, and obtain predictions of shaft motions showing a remarkable agreement with TC test stand rotordynamic measurements [5-7].

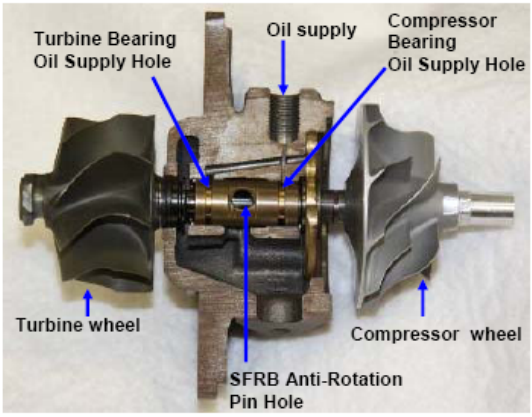

Fig. 1 Cutaway of passenger vehicle turbocharger rotor supported on semi-floating ring bearing

Engine-induced forced motions easily excite a TC center housing through the IC exhaust gases connecting manifold, invariably flexibly mounted. San Andrés et al. [8] further refine the predictive tool by including TC casing motions, transmitted forces into the rotor through the lubricated bearings. Note that the time scales for rotor motions arising from shaft rotation at high speeds, typically above 2 kHz (120 krpm), and those induced by IC engine rotation (typically < 200 Hz) are vastly different; the later being much longer. Hence, a model performing the time domain integration of the RBS equations of motion needs to last long enough to capture changes occurring at low frequencies, and yet keep a sufficiently small time step to catch high frequency content (mainly synchronous) without any distortion or signal leakage. Ref. [8] shows TC response predictions agreeing well with test data that shows multiple frequency responses containing multiples of the ICE firing frequency, self-excitation of natural frequencies, and synchronous response. In most cases, the response amplitudes due to rotor imbalance are just a small fraction (20% or less) of the total amplitude of motion, quite rich in frequency content.

Linear rotordynamic analyses, in general, predict natural frequencies and damping ratios from an eigenvalue analysis of the RBS equations of motion. Instabilities associated to the loss of damping are found at a certain threshold rotor speed; alas their effect on the system response is not quantified; i.e. the ensuing amplitude and frequency of the response are left unknown. A nonlinear analysis of the RBS can determine the threshold of instability as a bifurcation from a stable point into a limit cycle of single frequency, into a quasi-periodic orbit, or even into chaos. The bifurcations can be either stable if supercritical, or unstable if subcritical [10,11]. Subcritical bifurcations can show *hysteresis* where during rotor acceleration, the rotor onset speed of instability[1] is higher than the rotor speed at which the instability disappears during rotor deceleration. Refs. [3-7] and [12-16] present examples of this peculiar behavior. Wang and Khonsari [16] find that setting the appropriate lubricant temperature; ergo its viscosity, can control hysteresis in a lubricated RBS.

Internal and combined resonances are also common in non linear multiple degree of freedom mechanical systems. If at a certain operating speed, two (or more) of the natural frequencies are rational multiples of each other, an *internal resonance* may occur [17,18] A *combined resonance* couples two or more natural modes of a system and can cause an abrupt exchange of energy among the modes; at times large enough to determine mechanical system failure [18].

Holt *et al.* [3] and Schweizer and Sievert [19] report whirl frequency jumps and bifurcations in TC motion responses recorded during rotor speed up tests. Frequency domain analysis of the shaft motions displays, at a threshold rotor speed (Ω_b), a jump from a 1st subsynchronous whirl frequency (ω_1) to a 2nd higher (ω_2) frequency, and at times to a 3rd (lower) whirl frequency. Typically, shaft motions at the 2nd frequency (ω_2) are quite severe in amplitude [3]. Rotor motions at the 1st and 2nd whirl frequencies, subsynchronous in character, relate to instabilities of the inner film exciting the RBS conical and cylindrical-bending modes, respectively. The 3rd subsynchronous frequency, typical of fully-floating ring supported TCs, is due to the instability of the outer film that also excites a conical mode of whirl motion.

In TC operation practice, the frequency jump phenomenon, i.e. a sudden change from shaft motions with a dominant whirl frequency to motions with a higher whirl frequency and (even) larger amplitudes, results in increased levels of noise generation. Figure 2 shows two recorded instances of the whirl frequency jump phenomenon [20]. Note that increasing the oil inlet temperature from (a) 30°C to (b) 100°C decreases, from 108 krpm to 84 krpm, the shaft threshold speed (Ω_b) for frequency jump. Note, however, that the severity of whirl amplitude motions is somewhat larger for operation with a hotter lubricant.

This paper presents progress on quantifying the effects of oil inlet temperature and supply pressure, remnant imbalance distribution, and shaft (de)acceleration rates on the onset or the whirl frequency jump and on the ensuing severity of sub harmonic motions in a typical small passenger vehicle TC system. Frequency domain analysis of the predicted RBS motion responses reveals the complexity of the frequency jump phenomenon and points out to conditions for lower noise generation. Vistamehr [21] gives a complete account of the study, further detailing the effects of other parameters, not discussed here for brevity.

OVERVIEW OF ANALYSIS FOR PREDICTION OF TC ROTOR-BEARING SYSTEM RESPONSE

San Andrés *et al.* [2,4,8] develop the thermo-hydrodynamic fluid film bearing model predicting the (S)FRB static and dynamic forced performance characteristics (i.e. operating bearing clearances, effective film viscosity, fluid films temperature rise, ring and journal eccentricities, power losses, film flow rates, and dynamic fluid film force

[1] Here the word instability has a broad meaning, i.e., for example transition from an operating region with distinctive whirl frequencies into another region with also a unique set of whirl frequencies and associated amplitudes.

coefficients). The model accounts for shear thinning (non Newtonian) lubricant viscosity [22] and film bearing clearance variations due to shaft and ring thermal growths and rotating shaft centrifugal expansion. An empirically based temperature defect correlation delivers the shaft OD temperature at the turbine and compressor bearing locations [23].

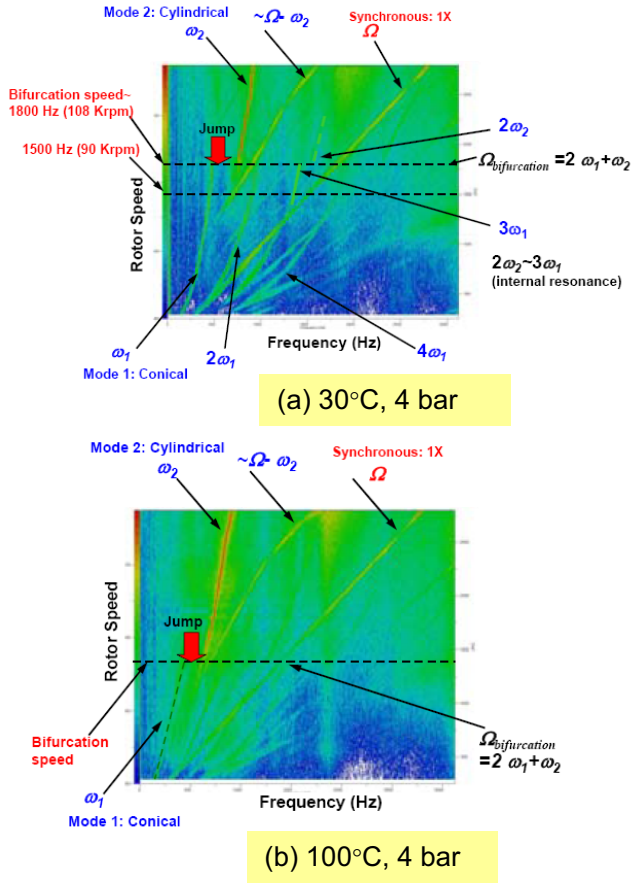

Fig. 2 Test data: waterfall of TC center housing acceleration. Whirl frequency jump noted. Lubricant supplied at 4 bar, oil inlet temperature varies. Ref. [20]

In the current analysis, the rotor bearing system (RBS) comprises of a TC rotor supported on a semi-floating ring bearing (SFRB), see Figure 1. The SFRB is a long and hollow bronze cylinder making two radial bearings, one at the compressor side and another at the turbine side. Each bearing comprises of an inner film between the shaft OD and ring ID and an outer film between the ring OD and casing ID. The compact design integrates thrust fluid film bearings, tapered pads type, on the axial ends of the hollow cylinder. A metal pin fits loosely into the SFRB preventing its rotation. Engine oil flows into the TC center housing to fill the outer films. Lubricant impinges directly into the compressor side bearing through a small hole, and a ½ moon groove or arched recess feeds lubricant to the turbine side outer film whilst creating a larger hydrostatic side (push) load than that on the compressor side bearing. Radial holes in the ring route lubricant from the outer films into the respective inner films. The lubricant is a light viscosity (multi-grade) mineral oil supplied at the nominal condition of 4 bar and 30°C inlet temperature.

Figure 3 depicts the TC rotor structural model consisting of 43 finite elements and the SFRB with 13 finite elements. A spring connecting the steel shaft to the brass ring denotes the inner film, and a spring connecting the ring to ground represents the outer film. As is common in rotor modeling, the turbine and compressor wheels are represented with added lumped mass and mass moments of inertia (polar and transverse) [24]. In the analysis, mass imbalance distributions follow common practice, for example at nose and/or back plane of compressor impeller, and at back and/or front faces of turbine wheel.

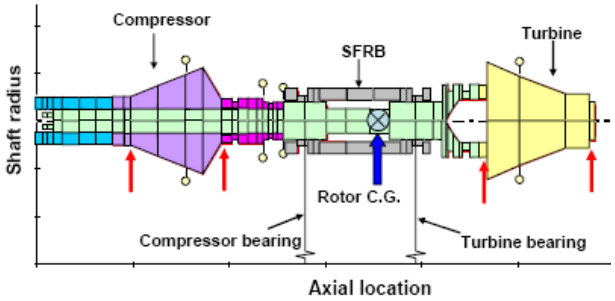

Fig. 3 TC structural finite element model of rotor and (semi) floating ring bearing

The fluid film bearing impedance model [2-8] is integral to the finite element (FE) Timoshenko beam rotor dynamics model for numerical prediction of the TC time transient forced response, linear and nonlinear [24,25]. Component mode synthesis [26] is used throughout the various analysis types available in the computational tool, including the time step numerical integration to obtain the nonlinear forced response of the RBS. A structural FE has left and right nodes, each with four degrees of freedom; two lateral displacements (x, y) and two rotations (φ_x, φ_y). The nonlinear rotordynamic analysis applies the instantaneous fluid film bearing reaction forces into the RBS equations of motion (EOM).

The floating ring bearing reaction forces are general functions of the geometry and operating conditions, such as shaft (Ω) and ring (Ω_R) rotational speeds, lubricant supply pressure and inlet temperature, viscosity of the inner and outer films, actual inner and outer film clearances affected by temperature gradients and centrifugal expansion, among others. The shaft and ring kinematics also determine the bearing forces, of course. In simplified form, the inner film ($\mathbf{F}_i$) and outer film ($\mathbf{F}_o$) reaction forces are expressed as [2]

$$\mathbf{F}_i = \begin{bmatrix} F_{X_i} \\ F_{X_i} \end{bmatrix} = \begin{bmatrix} f_X^i\left(x_J - x_R, y_J - y_R, \dot{x}_J - \dot{x}_R, \dot{y}_J - \dot{y}_R, \Omega, \Omega_R\right) \\ f_Y^i\left(x_J - x_R, y_J - y_R, \dot{x}_J - \dot{x}_R, \dot{y}_J - \dot{y}_R, \Omega, \Omega_R\right) \end{bmatrix} \quad (1a)$$

$$\mathbf{F}_o = \begin{bmatrix} F_{X_o} \\ F_{X_o} \end{bmatrix} = \begin{bmatrix} f_X^o\left(x_R - x_B, y_R - y_B, \dot{x}_R - \dot{x}_B, \dot{y}_R - \dot{y}_B, \Omega_R\right) \\ f_Y^o\left(x_R - x_B, y_R - y_B, \dot{x}_R - \dot{x}_B, \dot{y}_R - \dot{y}_B, \Omega_R\right) \end{bmatrix} \quad (1b)$$

where $(x_J, y_J)_{(t)}$, $(x_R, y_R)_{(t)}$ denote the dynamic displacements of the rotor and ring at the bearing location,

respectively, and $(x_B, y_B)_{(t)}$ represent the bearing casing or center housing specified motions. All rotor displacements are absolute, i.e. referenced to a fixed coordinate system. The equations of motions for the RBS operating with a varying rotor speed ($\Omega_{(t)}$) are [24]

$$\mathbf{M}\ddot{\mathbf{u}} + (\mathbf{C} + \Omega\mathbf{G_R})\dot{\mathbf{u}} + \mathbf{K}\,\mathbf{u} = \mathbf{F_S} + \mathbf{F_{imb}}(\Omega, \dot{\Omega}, t) + \mathbf{F_{ext}}(t) + \mathbf{F_B}(\mathbf{u}, \dot{\mathbf{u}}, \Omega) \quad (2)$$

where $\mathbf{u}^T = \sum \{x, y, \varphi_x, \varphi_y\}$ is the vector of generalized rotor and ring displacements, **M, K, C** and $\mathbf{G_R}$ denote the RBS mass, stiffness, damping and gyroscopic matrices. $\mathbf{F_S}$ is a vector of generalized static loads such as weight and hydrostatic pressure loads; $\mathbf{F_{ext}}(t)$ is a vector of specified external excitation forces and moments; and $\mathbf{F_{imb}}(\Omega, \dot{\Omega}, t)$ and $\mathbf{F_B}(\mathbf{u}, \dot{\mathbf{u}}, \Omega)$ represent the vectors of forces from a mass imbalance distribution and the fluid film bearings reaction forces, respectively. Above, the notation $\sum()$ intends to represent the collection of lateral and rotational displacements at each node of the FE model of the RBS.

The forces due to an imbalance mass (m) with offset displacement (e) acting at a distance (l) from a node are of the form [24]

$$\mathbf{F_{imb}}(\Omega, \dot{\Omega}, t) = \sum me \begin{bmatrix} \alpha_X & \alpha_Y & l\alpha_Y & -l\alpha_X \end{bmatrix}^T \quad (3)$$

where

$$\alpha_X = \Omega^2\cos(\theta) + \dot{\Omega}\sin(\theta), \alpha_Y = \Omega^2\sin(\theta) - \dot{\Omega}\cos(\theta), \text{ and } \theta = \int \Omega\, dt \quad (4)$$

The bearing reaction forces are only lateral (radial), not inducing local bending moments in the elastic system[2]. The bearing forces are written as

$$\mathbf{F_B}(\mathbf{u}, \dot{\mathbf{u}}, \Omega) = \sum \begin{bmatrix} F_{X_i} & F_{Y_i} & 0 & 0 \end{bmatrix}^T \text{ and } \sum \begin{bmatrix} F_{X_o} & F_{Y_o} & 0 & 0 \end{bmatrix}^T \quad (5)$$

for nodes with connections to the inner and outer films, respectively. Zero entries in Eqs. (4) and (5) denote null moments about the X and Y axes.

Note that the bearing reaction forces are highly nonlinear and calculated at each time step during the numerical integration of the RBS equations of motion. The rotordynamics analysis computational tool offers a choice of standard numerical algorithms for the integration of the EOMS recast in state-space form, i.e. as a set of first order differential equations. Presently, a *stiff* ODE *solver* [27] is selected since the code does not offer a choice for physically realistic initial condition, one consistent with the rotor elastic configuration under the action of the static load vector, for example. All analyses start with a zero initial state $(\mathbf{u} = \dot{\mathbf{u}} = \mathbf{0})$ that leads to rapid accelerations in the very first initial instants of motion as the numerical integration begins. Hence, the method chosen automatically sets a variable time step to avoid (obvious) numerical difficulties.

[2] The assumption is fully justified for short axial length fluid film bearings.

PREDICTIONS OF NONLINEAR ROTOR-BEARING SYSTEM RESPONSE

Predictions follow for the TC rotor response as the shaft accelerates with a 500Hz/s ramp rate from 30 krpm (0.5 kHz) to 240 krpm (4 kHz); and next, as it decelerates to 30 krpm (0.5 kHz). Seven seconds (7s) elapse for the shaft to reach the highest (lowest) shaft speed while accelerating (decelerating). In the numerical integration, the sampling rate is 10,000 samples/s (Δt = 0.1ms). For analysis, the predicted whole time domain response over 7s, 70,000 data points, is divided into segments of 2^{11}=2,048 points (time span of each segment ~102 ms) and applying the DFT (discrete Fourier Transform) to each time segment. The maximum frequency and frequency step (Δf) in the DFTs are 5,000Hz and 4.88 Hz, respectively. Ref. [21] lists pertinent physical dimensions and materials for the TC rotor and semi-floating ring. Below, predicted rotor response amplitudes are shown in dimensionless form with respect to the maximum physical displacement at the compressor end, as is common practice [4-8].

Baseline Case

The baseline analysis case accounts for nominal oil supply conditions (4 bar and 30°C), shaft acceleration rate at +/-500 Hz, and operation with a typical static -all in phase- imbalance distribution.

Figure 4(a) depicts the predicted waterfalls of TC shaft motion along the vertical direction (gravity plane). The synchronous response is labeled as 1X. Figure 4(b) shows the contour map of shaft motions; a yellow arrow marks the synchronous line. The amplitude of synchronous motions is quite small relative to those amplitudes at the distinctive subsynchronous whirl frequencies, labeled as ω_1 and ω_2, irrespective of the rotor acceleration, up or down.

From low shaft speeds up to 165 krpm (2.75 kHz), the TC rotor motions show mainly whirl at frequency ω_1. At shaft speed Ω_b=165 krpm there is a jump of the whirl motions with frequency ω_1 to motions with a second whirl frequency, ω_2, whose notorious influence persists to the highest shaft speed, 240 krpm (4 kHz). As the rotor decelerates from its top speed, whirl motions at ω_2 disappear at Ω_b=182 krpm (~3 kHz), with ω_1 suddenly appearing and enduring to the lowest shaft speed, 30 krpm (500 Hz).

Note that the motions with the 2nd whirl frequency persist over a longer shaft speed span during the ramp up motion (Ω>165 krpm) than when the rotor decelerates (Ω >182 krpm). The difference in speeds for whirl frequency jump while the shaft accelerates and decelerates is hereby termed as *hysteresis*, see its vivid details in the contour map of Fig. 4(b).

Figure 5 depicts the peak to peak (pk-pk) amplitude of shaft total motion during both rotor acceleration and deceleration. The total shaft motion, important for qualification of TCs, is an upper bound to the various components of motion: synchronous, subsynchronous and super synchronous. Note that the total amplitude of shaft

motion remains invariant whether the rotor accelerates or decelerates, ranging in between ~ 20% and 40% of the maximum allowed.

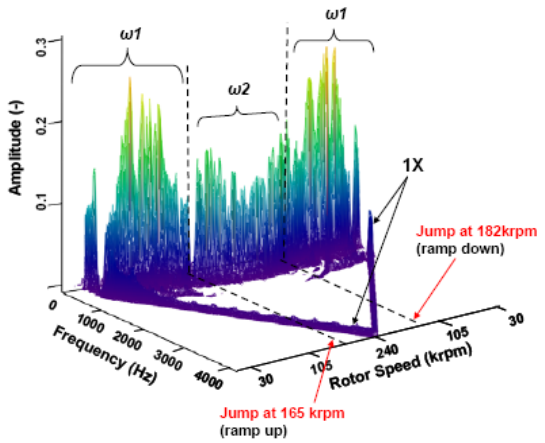

(a) 3D plot

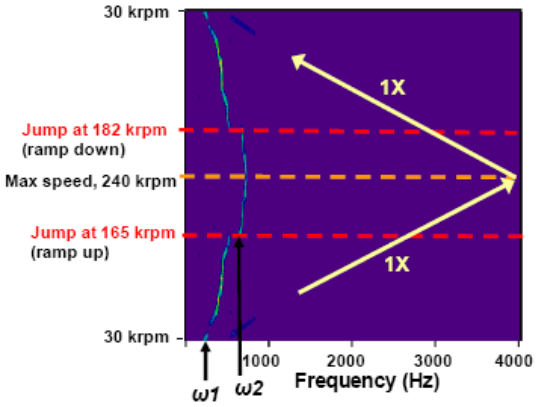

(b) contour map

Fig. 4 Waterfalls of predicted TC shaft motions at compressor end, vertical direction. Baseline case: shaft speed acceleration= +/- 500 Hz/s. Operation with static all-in-phase imbalance condition

Post-processing (filtering) of the predicted shaft motions shows distinctive features of the complicated shaft motions. Figure 6 depicts the RBS (subsynchronous) whirl frequencies versus shaft speed during rotor acceleration and deceleration. In both graphs, vertical lines denote the amplitude of a whirl motion at the particular frequency and rotor speed. Note the scale mark at 10% of maximum allowed for quantifying the whirl amplitudes. The diamond and triangle symbols denote the first (ω_1) and the second (ω_2) whirl frequencies, respectively. Filtering the frequency content of the nonlinear response predictions obtained at five locations in the RBS permits the construction of the (forced) mode shapes shown. Each whirl frequency determines a particular mode shape; a rotor conical mode for ω_1, and a cylindrical bending mode for ω_2.

As the rotor accelerates, Fig 6(a), the first whirl frequency (ω_1) increases from ~300 Hz to 670 Hz, and the second frequency (ω_2), suddenly appearing after Ω_b=165 krpm, ranges from ~820 Hz to 900 Hz. High amplitude motions correspond to the rotor conical whirl at ω_1, see amplitudes for frequencies from ~450 Hz to 600 Hz. Note that while the rotor accelerates and at speed Ω_b = 165 krpm (2,750 Hz), $5\omega_1$~$4\omega_2$ and $(3\omega_1+\omega_2) \sim \Omega_b$. Hence, at the speed location of the jump in whirl frequency, the interaction between an internal resonance and a combined resonance is the reason for the jump.

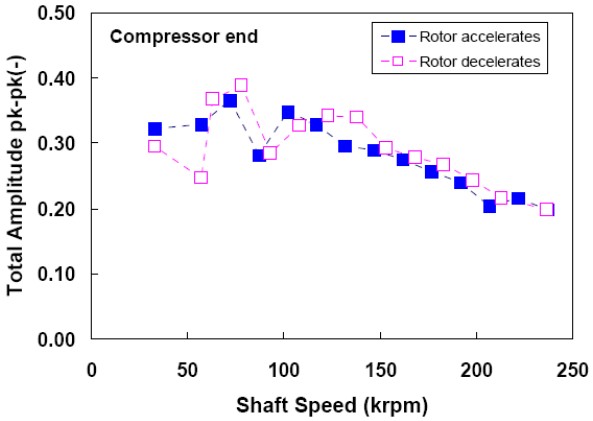

Fig. 5 Predicted TC total shaft motion (pk-pk) amplitude at compressor end during rotor acceleration (■ 500 Hz/s) and deceleration (□ -500 Hz/s). Operation with static all-in-phase imbalance condition

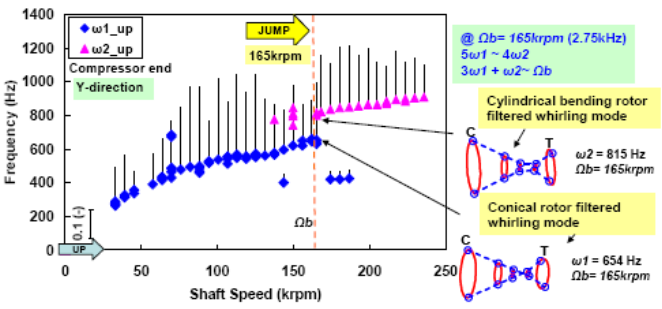

(a) rotor accelerates at 500Hz/s

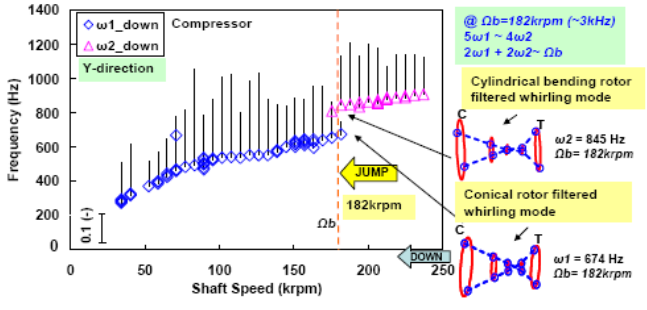

(b) rotor decelerates at -500Hz/s

Fig. 6 Predicted subsynchronous whirl frequencies and their motion amplitudes versus rotor speed. Baseline case: rotor acceleration at +/- 500 Hz/s. Normalized amplitudes at compressor end in vertical direction shown (scale included)

During rotor deceleration, Fig 6(b), the subsynchronous frequency regions appear at first to be similar. However, the frequency jump, from ω_2 into ω_1, occurs at a higher shaft

speed Ω_b =182 krpm (~3 kHz). Here, the combined resonance is $(2\omega_1+2\omega_2)$~Ω_b. Interestingly enough, the internal relation between ω_1 and ω_2 at Ω_b is identical to that during rotor acceleration, i.e. $5\omega_1$~$4\omega_2$.

As the rotor accelerates, Figure 7 overlays predicted damped natural frequencies (obtained from a linear [3]eigenvalue analysis) on the path of the subsynchronous whirl frequencies obtained from the nonlinear RBS time forced response. Subsynchronous whirl frequencies at low shaft speeds, <50 krpm, are at 50% of rotor speed denoting a characteristic instability of the inner film. As the shaft speed increases, the whirl frequency is not a fixed ratio of rotor speed. At Ω_b, the shaft speed of frequency jump, the rotor whirls with a frequency close to 25% of rotor speed. The 1st whirl frequency (ω_1) follows the conical mode (with SFRB also in a conical mode) up to shaft speeds around 80 krpm. Above 80 krpm, the rotor forced modes corresponding to whirl frequencies ω_1 and ω_2 resemble those predicted from the RBS linear eigenvalue analysis. However, the RBS predicted natural frequencies ω_1 and ω_2 are not close to the whirl frequencies from the forced response nonlinear model. Clearly, the linear rotordynamics analysis is representative only of small amplitude motions about the (static) equilibrium condition[4].

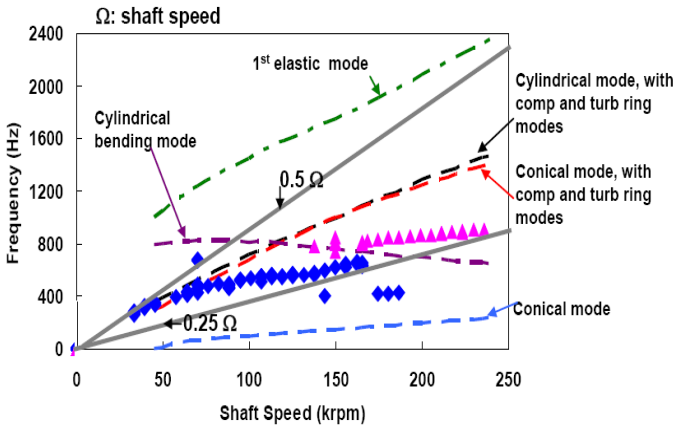

Fig. 7 Map of predicted damped natural frequencies from linear eigenvalue analysis and (nonlinear) subsynchronous whirl frequencies versus rotor speed. Baseline case: rotor acceleration=+500Hz/s. Operation with static all-in-phase imbalance condition

Effect of Oil Supply Pressure on Whirl Frequency Jump

For an operating condition with a reduced oil supply pressure, 66% from its nominal magnitude of 4 bar, Figure 8 depicts the TC whirl frequencies and associated displacement amplitudes versus shaft speed. Predictions show that the lesser oil inlet supply pressure reduces the shaft speed, at which the jump to the second whirl frequency (ω_2) occurs. That is, presently Ω_b = 118.8 krpm (1,980 Hz) while Ω_b = 165 krpm (2,750 Hz) for the 4 bar supply pressure condition.

This finding is consistent with TC shaft motion measurements in Ref. [19], where increasing the oil supply pressure from 1.5 bar to 3 bar delayed Ω_b from 45 krpm to 60 krpm. Incidentally, however, Ref. [3] reports that oil supply pressure, in a TC supported on fully floating ring bearings, has an insignificant effect on Ω_b. The discrepancy may be attributed to the unknown magnitude and distribution of rotor imbalance in the test TC.

Refer to Table 1 for the shaft speed (Ω_b) where the jump in whirl frequency, from ω_1 to ω_2, occurs while the rotor accelerates and decelerates. The table also provides the identified internal and combined resonances.

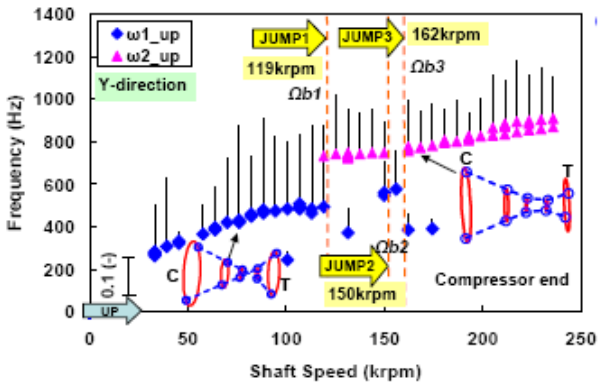

Fig. 8 Predicted subsynchronous whirl frequencies and their motion amplitudes versus rotor speed. Oil supply pressure reduced by 33%. Shaft acceleration= +500Hz/s. Normalized amplitudes in vertical direction shown at compressor end (scale included)

Effect of Oil Supply Temperature on Whirl Frequency Jump

For an operating condition with an increase in oil inlet temperature, 25°C above its nominal value, Figure 9 depicts the TC whirl frequencies and associated motion amplitudes versus shaft speed.

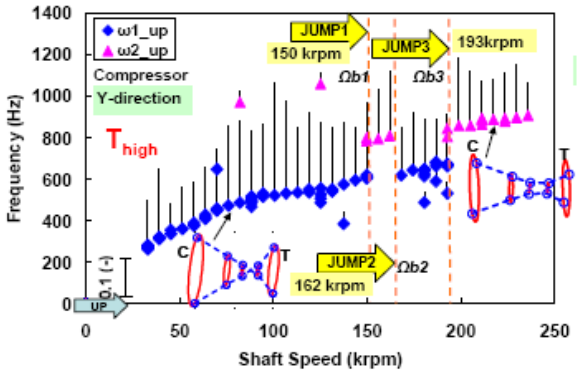

Fig. 9 Predicted subsynchronous whirl frequencies and their motion amplitudes versus rotor speed. Higher oil inlet temperature (T_{high}=55°C). Rotor acceleration = 500 Hz/s. Normalized amplitudes in vertical direction shown at compressor end (scale included)

[3] Note that the linear model natural frequencies may be different from those determined by the nonlinear model.

[4] In general, a (linearized system) eigenvalue analysis does not do well in predicting the actual natural frequencies in oil-lubricated TCs, whose notorious large amplitude subsynchronous whirl motions can only be determined by a full nonlinear RBS analysis. This simple fact makes relevant the present analysis.

In Fig.9, as the shaft accelerates, the larger oil inlet temperature produces a lower shaft speed (Ω_b) where there is a jump from the conical whirl mode at frequency ω_1 to the cylindrical bending mode at frequency ω_2. That is, compare presently Ω_b ~150 krpm (2.5 kHz) to Ω_b = 165 krpm (2,750 Hz) for the nominal temperature at 30°C. This result is consistent with the test data shown in Fig. 2. In Fig. 9 note the multiple frequency jumps as a result of the reduced oil viscosity (higher temperature). Refer to Table 1for the internal and combined resonances found.

Table 1. Main results from analysis of nonlinear response of a TC RBS. Internal and combined resonances between whirl frequencies ω_1 and ω_2 and threshold speed Ω_b. [21]

Case		Ω_b (Hz)	ω_1 (Hz)	ω_2 (Hz)	Internal resonance	Combined resonance
Baseline	(up)	2,750	654	815	$5\omega_1 \sim 4\omega_2$	$3\omega_1+\omega_2 \sim \Omega_b$
	(down)	3,030	674	845	$5\omega_1 \sim 4\omega_2$	$2\omega_1+2\omega_2 \sim \Omega_b$
Reduce oil supply pressure	(up)	1,980	493	732	$3\omega_1 \sim 2\omega_2$	$\omega_1+2\omega_2 \sim \Omega_b$
	(down)	2,000	508	732	$3\omega_1 \sim 2\omega_2$	$\omega_1+2\omega_2 \sim \Omega_b$
Increase oil inlet temperature	(up)	2,500	620	801	$4\omega_1 \sim 3\omega_2$	N/A
	(down)	3,030	645	840	$4\omega_1 \sim 3\omega_2$	$2\omega_1+2\omega_2 \sim \Omega_b$
Low shaft accel. +250Hz/s		2,500	635	840	$4\omega_1 \sim 3\omega_2$	N/A
Decel. -250Hz/s		2,620	645	811	$4\omega_1 \sim 3\omega_2$	N/A
High shaft accel. +750Hz/s		3,120	713	850	$6\omega_1 \sim 5\omega_2$	$2\omega_1+2\omega_2 \sim \Omega_b$
Decel. -750Hz/s		2,150	552	786	$3\omega_1 \sim 2\omega_2$	$\omega_1+2\omega_2 \sim \Omega_b$
Turbine back-plane out of phase Imb distribution	(up)	2,500	591	791	$4\omega_1 \sim 3\omega_2$	$3\omega_1+\omega_2 \sim \Omega_b$
	(down)	2,000	513	757	$3\omega_1 \sim 2\omega_2$	$\omega_1+2\omega_2 \sim \Omega_b$

N/A: resonance not found or not followed rational number combination
Baseline: oil inlet at 4 bar and 30 C, shaft speed ramp rate at 500 Hz/s.
▲ Up: rotor accelerates from 30 krpm (0.5 KHz) to 240 krpm (4 KHz). ▼ Down: rotor decelerates from 240 krpm to 30 krpm

Effect of Rotor Acceleration/Deceleration on Whirl Frequency Jump

The rate of rotor speed change (acceleration) clearly has a pronounced effect on the RBS response, linear or nonlinear. Predictions of rotor motion were obtained at various fixed shaft speeds as well as with various shaft speed ramp rates: 250 Hz/s, 500 Hz/s (baseline), and 750 Hz/s, see Ref. [21]. For brevity, results for the 750 Hz/s shaft speed ramp rate follow. Figure 10 depicts the whirl frequencies and their associated amplitudes versus shaft speed as the rotor accelerates and decelerates. In general, faster rotor acceleration delays the shaft speed Ω_b where a frequency jump occurs, i.e., from ω_1 to ω_2. A similar condition ensues as the rotor decelerates, i.e. the shaft speed at which the whirl frequency jumps, from ω_2 to ω_1, is much lower; and hence, the response *hysteresis* phenomenon is more marked. From the predictions, the difference between the rotor speeds Ω_b where a whirl frequency jump occurs during acceleration and deceleration is 7, 17 and 58 krpm for shaft speed ramp rates equaling 250, 500, and 750 Hz/s shaft peed ramp rates, respectively. Table 1 presents, for each acceleration condition, the shaft speed (Ω_b) where the jump in whirl frequency (ω_1 to/from ω_2) occurs, as well as the identified internal and combined resonances. In some instances, internal and combined resonances could not be easily discerned.

Prior (unpublished) work by San Andrés on the effect of shaft acceleration/deceleration on TC shaft motion response also shows that a higher rotor speed ramp rate, i.e. more rapid acceleration and deceleration, leads to a stronger hysteresis of the subsynchronous whirl motions (amplitude and frequency). This phenomenon is typical to subcritical bifurcations in nonlinear mechanical systems.

Effect of Imbalance Distribution on Whirl Frequency Jump – Out of phase condition

The baseline predictions refer to a static all-in-phase imbalance mass distribution. Presently, the same imbalance masses are kept, however their disposition on the turbine wheel has opposing angles at its front and back planes. This imbalance condition induces a bending moment on the turbine. See Ref. [21] for predictions related to other likely combinations of imbalance distributions.

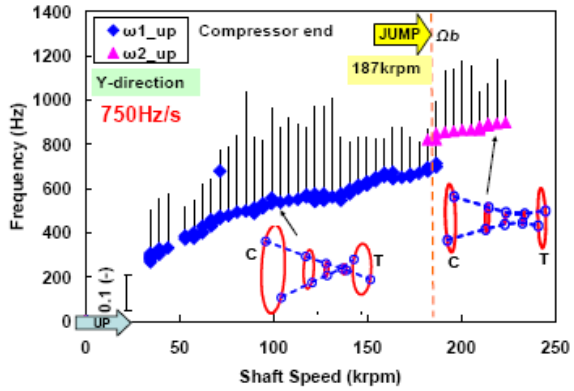

(a) rotor accelerates at 750Hz/s

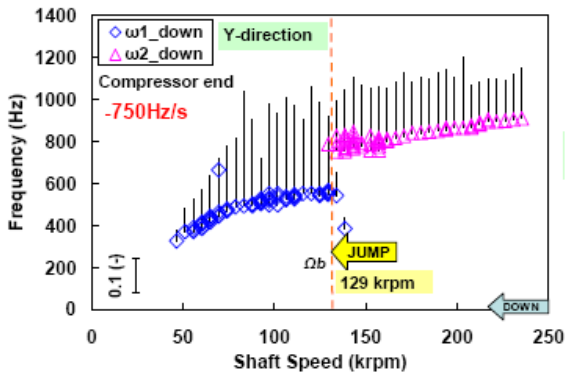

(b) rotor decelerates at -750Hz/s

Fig. 10 Predicted subsynchronous whirl frequencies and their amplitudes of motion versus rotor speed. Operation with a faster rotor acceleration = +/- 750Hz/s. Normalized amplitudes in vertical direction shown at compressor end (scale included)

Figure 11 depicts the subsynchronous whirl frequencies and their associated amplitudes versus shaft speed for the turbine back-plane out-of-phase imbalance condition. All other conditions are nominal and the TC rotor accelerates. Note that, relative to the response obtained for the all-in-phase imbalances (see Fig. 6); presently, the shaft speed Ω_b at which there is a whirl frequency jump decreases as the rotor accelerates. Most noticeably, however, motions with the second whirl frequency (ω_2) disappear altogether shortly after the threshold speed Ω_b. See Table 1 for the internal and combined resonances identified.

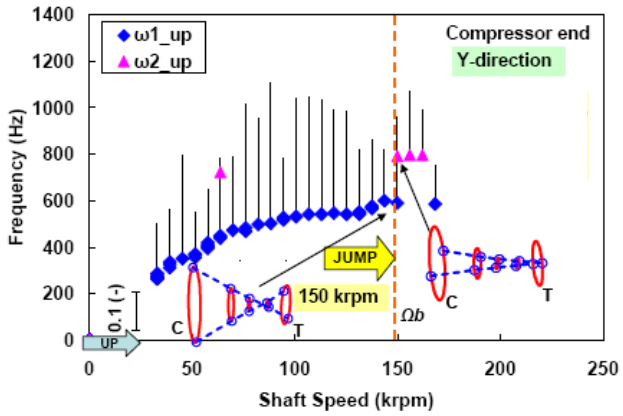

Fig. 11 Predicted subsynchronous whirl frequencies and their amplitudes of motion versus rotor speed. Operation with turbine back-plane out-of-phase imbalance. Rotor acceleration = 500Hz/s. Operation with turbine out-of-phase imbalance. Normalized amplitudes in vertical direction shown at compressor end (scale included)

Figure 12 shows the total amplitude of shaft for the turbine back plane out-of-phase imbalance condition. Note at rotor speeds above ~160 krpm the total motion is just < 10% of the physical limit, thus showing eminently a synchronous rotor response, i.e., a linear system response characteristic. To realize the major differences, compare the present total motion with that for the baseline, see Figure 5, which accounts for an all-in-phase imbalance condition. Due to the reduced amplitudes of motion and a notorious absence of subsynchronous whirl motion (no obvious nonlinearities), the out-of-phase imbalance distribution is particularly noteworthy.

Effect of Imbalance Amount on Whirl Frequency Jump – Out of phase condition

A further prediction with twice as large mass imbalances should reveal if the absence of the subsynchronous whirl motions persists within the high speed range operation. Figure 13 depicts the existence of a single subsynchronous whirl frequency with moderate amplitude, while Figure 14 shows the amplitude of total motion as synchronous for most of the operating speed range. Increasing the imbalance mass ameliorates the effects of the nonlinearities, and in essence produces a RBS response free of sub harmonic whirl over a wide range of rotor speeds. Alas this observation can not be generalized for turbocharger RBS. Nonetheless, it is well known that large imbalances effectively suppress lubricated bearing self-excited instabilities [28].

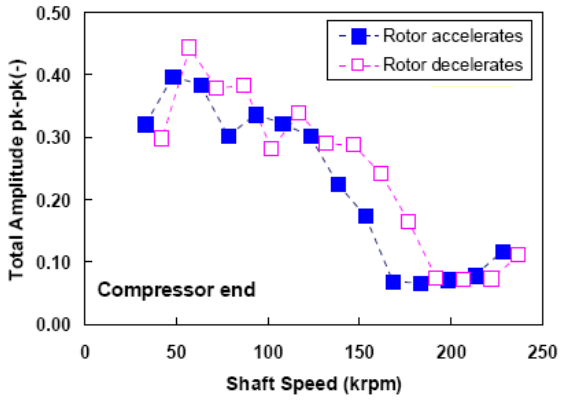

Fig. 12 Predicted TC total shaft motion (pk-pk) amplitude at compressor end during rotor acceleration (500 Hz/s) and deceleration (-500 Hz/s). Operation with turbine out-of-phase imbalance condition

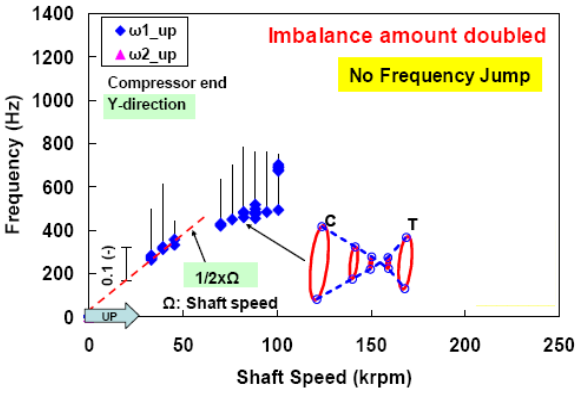

Fig. 13 Predicted subsynchronous whirl frequency and amplitude of motion versus rotor speed. Rotor acceleration = 500Hz/s Operation with turbine out-of-phase imbalance; twice amount of imbalance in all planes

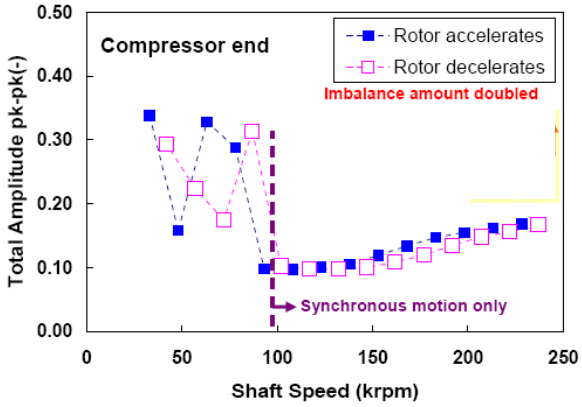

Fig. 14 Predicted TC total shaft motion (pk-pk) amplitude at compressor end during rotor acceleration (500 Hz/s) and deceleration (-500 Hz/s). Operation with turbine out-of-phase imbalance; twice amount of imbalance in all planes

Incidentally, to the authors' knowledge, (proprietary) test data also evidences the suppression of high amplitude whirl motions for operation with larger imbalances. Needless to say, operation without any whirl frequency generates little noise.

CONCLUSIONS

Rotor-bearing system motions in engine oil lubricated turbochargers (TCs) are extraordinarily complex. Typically, not just one but various subsynchronous whirl frequency motions, typically of large amplitude, appear at distinct shaft speeds. These motions are a result of the nonlinearity and hydrodynamic instability of either the inner film, or the outer film, or both films in the compressor side bearing and/or the turbine side bearing. At a certain threshold rotor speed (Ω_b), certain operating conditions cause a jump in whirl frequency and its associated rotor motions. Both whirl frequencies are subsynchronous; the lowest is associated to a conical rotor motion mode shape; while the second, at a higher frequency, is related to a rotor cylindrical-bending mode shape. When the whirl frequency jumps, the rotor deflected mode of motion changes drastically thus generating more noise level in automotive TCs.

In an effort to improve TC dynamic forced performance by reducing noise levels, nonlinear rotordynamic predictions are obtained for a small TC supported on a semi-floating ring bearing (SFRB). The TC unit operates to a very high speed, max. 240 krpm (4 kHz), and due to is small size and inertia, can accelerate or decelerate very fast, max. 1 kHz/s. Variations in oil supply conditions (pressure and temperature), operation with increasing shaft rotation acceleration or deceleration, as well as a number of mass imbalance configurations, determine distinct rotor motions that evidence the jumps in whirl frequency at different threshold rotational speeds while the TC rotor accelerates. Most notably, there is a pronounced hysteresis phenomenon, since as the rotor decelerates from its max. speed, the threshold speed for the jump in whirl frequency is markedly distinct than when the rotor accelerates. Operation with the fastest rotor acceleration (deceleration) rate, at 1 kHz/s, produces the strongest hysteresis.

At low shaft speeds (< 100 krpm) and at high speeds (> 200 krpm), predicted rotor whirl motions, sub harmonic in character, are similar in both frequency and amplitude content, for most considered operating conditions, with one exception. A rotor imbalance distribution known as turbine back plane-out-of-phase produces stable rotor motions, free of subsynchronous whirl, while operating at high shaft speeds. For the various operating conditions, differences in rotor motion response, amplitudes and frequency content, are most apparent in the shaft speed range 100 krpm to 200 krpm, which encloses the threshold speed Ω_b, hence revealing the jump frequency phenomenon.

Relative to operation at nominal conditions (4 bar supply pressure and 30 C inlet oil temperature, and 500 Hz/s ramp speed rate), predictions show that reducing the oil supply pressure, and to a lesser extent increasing the oil inlet temperature, brings the whirl frequency jump to occur at a lower threshold speed (Ω_b). Hence, TC operation becomes noisier[5] for operation at higher shaft speeds, $\Omega > \Omega_b$.

In most cases, at the rotor speed Ω_b where a whirl frequency jumps there is an *internal resonance* between the two whirl frequencies, ω_1 and ω_2. That is the ratio ω_1/ω_2 is a rational number. At the threshold speed there are also *combined resonances*, i.e. $A\omega_1 + B\omega_2 = \Omega_b$, combinations of low integers (A, B=1,2,3) of the whirl frequencies add to the shaft speed. The internal resonances are the same during rotor acceleration and deceleration. The internal and combined resonances are responsible for energy exchanges between the rotor modes of motion in a nonlinear system.

The rotor mass imbalance distribution affects the rotor whirl motions -amplitude and frequency; and hence, the shaft speed where a whirl frequency jumps and the internal resonances between the whirl frequencies. In addition, imbalance distribution also affects the degree of hysteresis in the RBS nonlinear response. One particular configuration, turbine back plane-out-of-phase produces stable rotor motions, not exacerbated by inducing larger imbalances.

The nonlinear predictions agree (qualitatively) well with test data reported in the literature. See Ref. [21] for TC motion predictions and discussion related to other mass imbalance distributions as well as for changes in bearing length. The aim in Ref. [21] is to assess the imbalance condition that results in the smallest amplitudes of rotor motion and without excitation of subsynchronous whirl motions.

ACKNOWLEDGEMENTS

The technical guidance of Dr. Kostandin Gjika, Engineering and Technology Fellow at Honeywell Turbo Technologies (HTT) is recognized. Approval from HTT to publish this paper received on January 24, 2010.

The first author is the sole responsible for the technical material hereby presented. Dr. San Andrés also supported financially Ms. Arian Vistamehr to conduct the research and complete her M.S. thesis [21].

REFERENCES

1. Haller, C. L., Killinger, A. G., and Smith, L. A., 1995, "Methods to Reduce Diesel Engine Exhaust Emissions at Established Installations to Comply with the Clean Air Act," ASME/ ICE Journal, **4**, pp.75-84.
2. San Andrés, L., and Kerth, J., 2004, "Thermal Effects on the Performance of Floating Ring Bearings for Turbochargers," Proc. of the Inst. of Mech. Eng., Part J, J. Eng. Tribol., **218**(5), pp. 437-450.
3. Holt, C., L. San Andrés, S. Sahay, P. Tang, G. LaRue, and K. Gjika, 2005, "Test Response and Nonlinear Analysis of a Turbocharger Supported on Floating Ring Bearings," ASME J. Vib. Acoust., **127**, pp. 107-115.
4. San Andrés, L., J.C. Rivadeneira, K. Gjika, C. Groves, and G. LaRue, 2007, "Rotordynamics of Small Turbochargers Supported on Floating Ring Bearings – Highlights in Bearing

[5] Post-processing of the predicted rotor dynamic motions as sound (waves with distinct amplitude and frequency) reveals this fact. Unfortunately, playing sound is not yet possible in an archival publication.

Analysis and Experimental Validation," ASME J. Trib, **129**, pp. 391-397.
5. San Andrés, L., Rivadeneira, J. C., Chinta, M., Gjika, K., and LaRue, G., 2007, "Nonlinear Rotordynamics of Automotive Turbochargers: Predictions and Comparisons to Test Data," ASME J. Eng. Gas Turb. Power, **129**, pp. 488-493.
6. San Andrés, L., J.C. Rivadeneira**,** K. Gjika, C. Groves, and G. LaRue, 2007, "A Virtual Tool for Prediction of Turbocharger Nonlinear Dynamic Response: Validation against Test Data," ASME J. Eng. Gas Turb. Power, **129,** pp. 1035-1046.
7. Gjika, K., Groves, C., San Andrés, L., and G. LaRue, 2007, "Nonlinear Dynamic Behavior of Turbocharger Rotor-Bearing Systems with Hydrodynamic Oil Film and Squeeze Film Damper in Series: Prediction and Experiment," Proc. of the 21st Biennial Conference on Mechanical Vibration and Noise, Las Vegas, NV, September 4-7, Paper No. DETC 2007-34136.
8. San Andrés, L., Maruyama, A., Gjika, K., and Xia, S., 2010, "Turbocharger Nonlinear Response with Engine-Induced Excitations: Predictions and Test Data," ASME J. Eng. Gas Turb. Power, **132, 032502** (ASME Paper GT2009-59108)
9. Macinnes, H., and Johnston, A., 1982, "Comparison of Power Loss Between Full Floating and Semi-Floating Turbocharger Bearings," Proceedings of IMechE Conference on Turbocharging and Turbochargers, London, Paper C46/82, pp. 157–164
10. Noah, S., and Sundararajan, P., 1995, "Significance of Considering Nonlinear Effects in Predicting the Dynamic Behavior of Rotating Machinery," J. Vibration and Control, **1**, pp. 431-458.
11. Yamamoto, T., and Ishida, Y., 2001, Linear and Nonlinear Rotordynamics: A Modern Treatment with Applications, Wiley, New York.
12. Pinkus, O., 1956, "Experimental Investigation of Resonant Whip," Trans. ASME, **78**, pp. 975-983.
13. Shaw, J., and Shaw, S. W., 1990, "The Effect of Unbalance on Oil Whirl," Nonlinear Dynamics, **1**, pp. 293-311.
14. Muszynska, A., 1998, "Transition to Fluid-Induced Stability Boundaries Self-Excited Vibrations of a Rotor and Instability Threshold 'Hysteresis'," Proc. of ISROMAC-7, The 7th International Symposium on Transport Phenomena and Dynamics of Rotating Machinery, February, Honolulu, HI, pp. 775-784.
15. Naranjo, J., C. Holt, and L. San Andrés, 2001, "Dynamic Response of a Rotor Supported in a Floating Ring Bearing, 1st International Conference in Rotordynamics of Machinery, ISCORMA1, Lake Tahoe, NV, Paper 2005.
16. Wang, J. K., and Khonsari, M. M., 2006, "On the Hysteresis Phenomenon Associated with Instability of Rotor-Bearing Systems," ASME J. Trib,, **128**, pp. 188-196.
17. Nayfeh, A. H., and Balachandran, B., 1989, "Modal Interactions in Dynamical and Structural Systems," ASME Appl Mech Rev, **42**, pp.175-201.
18. Nayfeh, T. A., Asrar, W., and Nayfeh, A. H., 1992, "Three-Mode Interactions in Harmonically Excited Systems with Quadratic Nonlinearities," Nonlinear Dynamics, **3**, pp. 385-410.
19. Schweizer, B., and Sievert, M., 2009, "Nonlinear Oscillations of Automotive Turbocharger Turbines," J. Sound Vib., **321**, pp. 955-975.
20. Gjika, K., 2004, "Bearing Systems Behavior - Subsynchronous Vibration and Relationship with Noise: Applications to PV Turbochargers," Proprietary, Honeywell Turbo Technologies, TLV France.
21. Vistamehr, A., 2009, "Analysis of Automotive Turbocharger Nonlinear Vibrations Including Bifurcations," M.S. Thesis, Texas A&M University, Mechanical Engineering, College Station, TX, December.
22. Taylor, R. I., 1999, "The Inclusion of Lubricant Shear Thinning in the Short Bearing Approximation," Proc. Inst. Mech. Engrs, **213** (1), pp. 35-46.
23. San Andrés, L., 2007, Analysis of TC Rotor Temperature Telemetry Data, Proprietary Technical Report #41 to Honeywell Turbocharging Technology, Texas A&M University, College Station, TX, May.
24. Childs, D., 1993, Turbomachinery Rotordynamics: Phenomena, Modeling, & Analysis, John Wiley & Sons, Inc., NY, Chapter 4.
25. XLTRC^2 Rotordynamics Software Suite v.2.22, 2008, Turbomachinery Laboratory, Texas A&M University, College Station, TX.
26. Craig, R., 1981, Structural Dynamics, John Wiley & Sons, Inc., NY, Chapter 11.
27. IMSL Fortran Library V 6.0 - February 2007 (Gear-Stiff Solver)
28. San Andrés, L., 2009, Modern Lubrication, Lecture Notes #5. http://rotorlab.tamu.edu/Tribgroup, [accessed November 2009]